The Astronomical Journal, 133:2892–2897, 2007 June

THREE-DIMENSIONAL SPECTROSCOPY OF BLUE COMPACT GALAXIES: DIAGNOSTIC DIAGRAMS

Ismael Martínez-Delgado,[1] Guillermo Tenorio-Tagle,[2] Casiana Muñoz-Tuñón,[1]
Alexei V. Moiseev,[3] and Luz M. Cairós[4]
Received 2006 December 6; accepted 2007 February 15

ABSTRACT

Here we present the analysis of three-dimensional spectroscopic data of three blue compact galaxies (Mrk 324, Mrk 370, and III Zw 102). Each of the more than 22,500 spectra obtained for each galaxy has been fitted by a single Gaussian from which we have inferred the velocity dispersion (σ), the peak intensity ($I_{\rm peak}$), and the central wavelength (λ_c). The analysis shows that the σ versus $I_{\rm peak}$ diagrams look remarkably similar to those obtained for giant extragalactic H II regions. They all present a supersonic narrow horizontal band that extends across the entire range of intensities and that results from the massive nuclear star-forming regions of each galaxy. The σ versus $I_{\rm peak}$ diagrams also present several inclined bands of lower intensity and an even larger σ arising from the large galactic volumes that surround the main central emitting knots. We also show that the σ versus λ_c and λ_c versus $I_{\rm peak}$ diagrams are powerful tools that are able to unveil the presence of high- and low-mass stellar clusters, and thus allow for the possibility of inferring the star formation activity of distant galaxies even if they are not spatially resolved.

Key words: galaxies: dwarf — galaxies: individual (Markarian 370, Markarian 324, III Zwicky 102) — galaxies: kinematics and dynamics — galaxies: starburst

1. INTRODUCTION

High-resolution panoramic spectroscopy with good spatial and spectral resolution is known to be a powerful tool for studying the kinematics of ionized nebulae, as it leads to a simultaneous mapping, at seeing-limited resolution, of a particular emission line over the whole nebula. However, this can easily lead to several tens of thousands of spectra, making it difficult to issue a detailed and/or global interpretation of the data. An analysis procedure that has proven to be simple and powerful results from fitting a single Gaussian to each of the resultant emission-line profiles (see Muñoz-Tuñón 1994; Muñoz-Tuñón et al. 1995), regardless of the actual degree of asymmetry or splitting in the line profiles. The fit conserves the flux of the line profile, and thus, lower intensity but broader lines would result from the most asymmetric or strongly split line profiles. From the resultant fits one can derive the velocity dispersion (σ) and the peak intensity ($I_{\rm peak}$) of the fitted lines, as well as their central wavelength (λ_c). Such a method, when applied to giant extragalactic H II region (GHIIR) data, leads to two distinct regions in the σ versus $I_{\rm peak}$ diagram (see Muñoz-Tuñón et al. 1996): a supersonic ($\sigma > c_{\rm H\,II}$), relatively narrow horizontal band with all possible peak intensity values, and a second region populated by lower intensity points presenting even larger supersonic σ-values, which crowd along multiple inclined bands. For the case of GHIIRs it has been shown (see Muñoz-Tuñón 1994; Muñoz-Tuñón et al. 1996; Sabalisck et al. 1995; Fuentes-Masip et al. 2000; see also Telles et al. 2001 for the case of H II galaxy data) that the horizontal band is formed by data with truly Gaussian profiles arising mainly from the brightest portions of the nebula, i.e., from the small regions that enclose groups or clusters of stars. The inclined lower intensity and highly supersonic bands, on the other hand, emanate from multiple photoionized shells that surround the star-forming centers and are likely to result from the stellar mechanical energy impact on the ISM, and thus from single-Gaussian fits to highly asymmetric or strongly split lines. The analysis of the σ versus $I_{\rm peak}$ diagram for GHIIRs in nearby galaxies (closer than 1 Mpc) was then proposed as an excellent tool to determine their degree of evolution on kinematic bases (Muñoz-Tuñón et al. 1996). Here we extend the analysis to blue compact galaxies (BCGs) at even larger distances and show that they experience a similar dynamical evolution (i.e., their σ vs. $I_{\rm peak}$ diagrams look very much like those of GHIIRs). We further extend our analysis by looking also at the σ versus λ_c and λ_c versus $I_{\rm peak}$ diagrams and show them as ideal tools to distinctly unveil the presence of high- and low-mass stellar clusters.

Section 2 provides a short description of the observations. Section 3 contains a detailed analysis of the data by means of the diagnostic diagrams proposed, and § 4 gives a summary and a discussion of our findings.

2. THE OBSERVATIONS

We used the 6 m Big Telescope Alta-azimuthal (BTA) of the Special Astrophysical Observatory (SAO) in Nizhnij Arkhyz (Russia), equipped with the multimode focal reducer SCORPIO[5] in the scanning interferometer Fabry-Perot (IFP) observational mode (see Afanasiev & Moiseev 2005), for observations of three BCGs: Mrk 370, III Zw 102, and Mrk 324. SCORPIO is provided with an EEV 42-40 CCD array of 2048×2048 pixels, with an instrumental scale of $0.18''$ pixel^{-1}. A set of interference filters centered at the Hα line, covering an interval of systemic velocities that range from -200 to 10,000 km s^{-1}, is used in the IFP observational mode. The IFP offers two configurations, depending on the interference order: in our case at the Hα line, IFP260 (at interference order 235) and IFP500 (at interference order 501). Our observation runs were performed using the IFP500 mode, which offers a better spectral resolution in the Hα emission line.

[1] Instituto de Astrofísica de Canarias, E-38200 La Laguna, Tenerife, Canary Islands, Spain; idelgado@iac.es, cmt@iac.es.
[2] Instituto Nacional de Astrofísica, Óptica y Electrónica, 72000 Puebla, Mexico; gtt@inaoep.mx.
[3] Special Astrophysical Observatory, 369167 Nizhnij Arkhyz, Russia; moisav@sao.ru.
[4] Astrophysikalisches Institut Potsdam, D-14482 Potsdam, Germany; luzma@aip.de.

[5] See http://www.sao.ru/hq/lsfvo/devices/scorpio/scorpio.html.

TABLE 1
LOG OF THE OBSERVATIONS

Galaxy (1)	R.A. (J2000.0) (2)	Decl. (J2000.0) (3)	Linear Scale (pc arcsec^{-1}) (4)	t (s) (5)	PSF (arcsec) (6)	$V_{\rm H\,I}$ (km s^{-1}) (7)	D (Mpc) (8)
Mrk 370	02 40 29.0	+19 17 50	52	4680	1.7	790[a]	10.85
III Zw 102	23 20 30.1	+17 13 32	110	6480	1.8	1626[a]	22.71
Mrk 324	23 26 32.8	+18 15 59	108	4320	1.6	1600[a]	22.43

NOTE.—Units of right ascension are hours, minutes, and seconds, and units of declination are degrees, arcminutes, and arcseconds.
[a] Systemic velocity, from H I observations, corrected to the Local Group velocity centroid taken from Thuan & Martin (1981).

The output from the IFP results in a three-dimensional data cube, with x and y being the spatial plane and z the wavelength sampling or ethalon step; in the case of the IFP500 mode, this translates into 32–40 channels. The original data cube dimensions were (522, 522, 36), although for our analysis we reduced the size to (150, 150, 36). The free spectral range (FSR) was 13 Å, enough to sample the Hα line, which was scanned with a spectral sampling of 0.7 Å ($\approx$32 km s^{-1}). A binning of 4×4 pixels was applied in the spatial directions in order to reduce the time exposure and improve the signal-to-noise ratio of the final data cube, resulting in a final spatial scale of 0.7″ pixel^{-1}. The instrumental width taken from a fitting of the calibration lamp data cube was $\sigma_{\rm inst} = 20 \pm 3$ km s^{-1}. Table 1 lists a log of the observations together with some data about the galaxies: column (1) gives the name of the object, columns (2) and (3) show the coordinates (from NED[6]), column (4) shows the linear scale for each galaxy, column (5) lists the total time exposure of the observations, column (6) gives the seeing conditions, column (7) shows the systemic velocity of each galaxy, and column (8) gives the distance in megaparsecs. Each of our SCORPIO-trimmed data cubes contains a total of 22,500 spectra from an area of $\sim$3 arcmin^2. The bulk of the data thus require automatic techniques of analysis to extract the full power of the three-dimensional spectroscopy. For each of the three galaxies, their Hα emission lines in each pixel were fitted by single Gaussians to obtain their $I_{\rm peak}$, σ, and λ_c, as described in Muñoz-Tuñón et al. (1995, 1996). The velocity dispersion is given in kilometers per second and was corrected for the instrumental and thermal broadening ($\sigma^2 = \sigma^2_{\rm obs} - \sigma^2_{\rm inst} - \sigma^2_{\rm th}$). We then used MoisSoft, the software package designed for the manipulation of SCORPIO IFP spectral line data cubes. For a detailed explanation about the data reduction procedure, see Moiseev (2002).

3. THREE-DIMENSIONAL SPECTROSCOPY OF BCDs

3.1. *Mrk 324*

Mrk 324 is a galaxy classified as a blue compact dwarf (BCD; see Thuan & Martin 1981) and is included as a nucleated BCD in the morphological classification of Cairós et al. (2001), as it is basically powered by a luminous central knot. The star formation history of the galaxy fits well with an instantaneous star formation law with a Salpeter IMF ($\alpha = 2.35$) and a range of masses $1\ M_\odot \leq M \leq 100\ M_\odot$, in which a central knot of 4.4 Myr and $1.4 \times 10^5\ M_\odot$ in stars dominates 95% of the emission flux of the galaxy (see Martínez-Delgado et al. 2006).

Figure 1 (*top row*) shows the results from the single-Gaussian fit to the full Hα SCORPIO data set in the σ versus $I_{\rm peak}$, σ versus λ_c, and λ_c versus $I_{\rm peak}$ diagrams for Mrk 324. The top right panel shows the Hα image of the nucleated galaxy (see Cairós et al. 2001) obtained at the NOT 2.52 m telescope of the Observatorio del Roque de Los Muchachos (ORM) in La Palma (Spain). The resemblance of the σ versus $I_{\rm peak}$ diagram to those of GHIIRs is remarkable. It presents a horizontal band that limits the values of σ to supersonic values ($\sigma \geq 20$ km s^{-1}), and a bunch of low-intensity points at even higher σ-values, which delineate a triangular structure above the horizontal band. If one selects from the σ versus $I_{\rm peak}$ diagram the highest intensity data points, those belonging to the horizontal band (see Fig. 1, *middle row*), the data points in the σ versus λ_c diagram appear clumped at a given λ_c ($\sim$6598.2 Å), which implies that they all arise from a very similar location in the galaxy and that they all belong in principle to a single entity. Note, however, that this is not exactly coincident with the rest wavelength of the galaxy (marked in the λ_c plots with a red line; see Fig. 1). The selected points in the λ_c versus $I_{\rm peak}$ diagram also define a pointed structure toward high-intensity values. These points in the emission-line peak intensity maps (*middle row, last panel*) display their location in the galaxy, which indeed coincides with a major burst of star formation in Mrk 324, with an estimated mass in stars of $\sim 4 \times 10^5\ M_\odot$ and an age of about 4.4 Myr (see Martínez-Delgado 2005; Martínez-Delgado et al. 2006), causing an H II region with a radius of $\sim$250 pc. On the other hand, the data belonging to the inclined bands with a higher velocity dispersion and a lower intensity in the σ versus $I_{\rm peak}$ diagram (see Fig. 1, *bottom row*) appear well scattered in λ_c and arise from a large-scale (600 pc in thickness) expanding rim that surrounds the central emitting knot, as shown in the bottom right panel. The insets in the last column of Figure 1 display the Hα line and its single-Gaussian fit at various locations in the galaxy. As in GHIIRs, the data corresponding to the horizontal band in the σ versus $I_{\rm peak}$ diagram lead to the highest intensity true Gaussian profiles, while the profiles fitted to lower intensity and larger σ data points, arising from the outer expanding rim, are fits to asymmetric and/or double-peak line profiles. Figure 1 shows the quality of typical line profiles from each of the regions, displaying their intensity, central wavelength, and σ-values.

3.2. *Mrk 370*

This BCD galaxy belongs to the "chained" morphological type (see Cairós et al. 2001), in which the star formation takes place along a privileged direction. It follows the same star formation law as Mrk 324, with 25 young and massive exciting clusters hosted over an underlying stellar component with ages larger than 5 Gyr (see Cairós et al. 2002). The clusters have an average age of 6.6 Myr with a dispersion of 0.9 Myr, suggesting a coeval and global star formation event. For the ones located in the inner nuclear region, the stellar mass content reaches up to several $10^5\ M_\odot$ (see Martínez-Delgado et al. 2006).

Figure 2 displays similar diagnostic diagrams for Mrk 370. The top right panel shows the Hα image of the chained galaxy

[6] The NASA/IPAC Extragalactic Database is operated by the Jet Propulsion Laboratory, California Institute of Technology, under contract with the National Aeronautics and Space Administration.

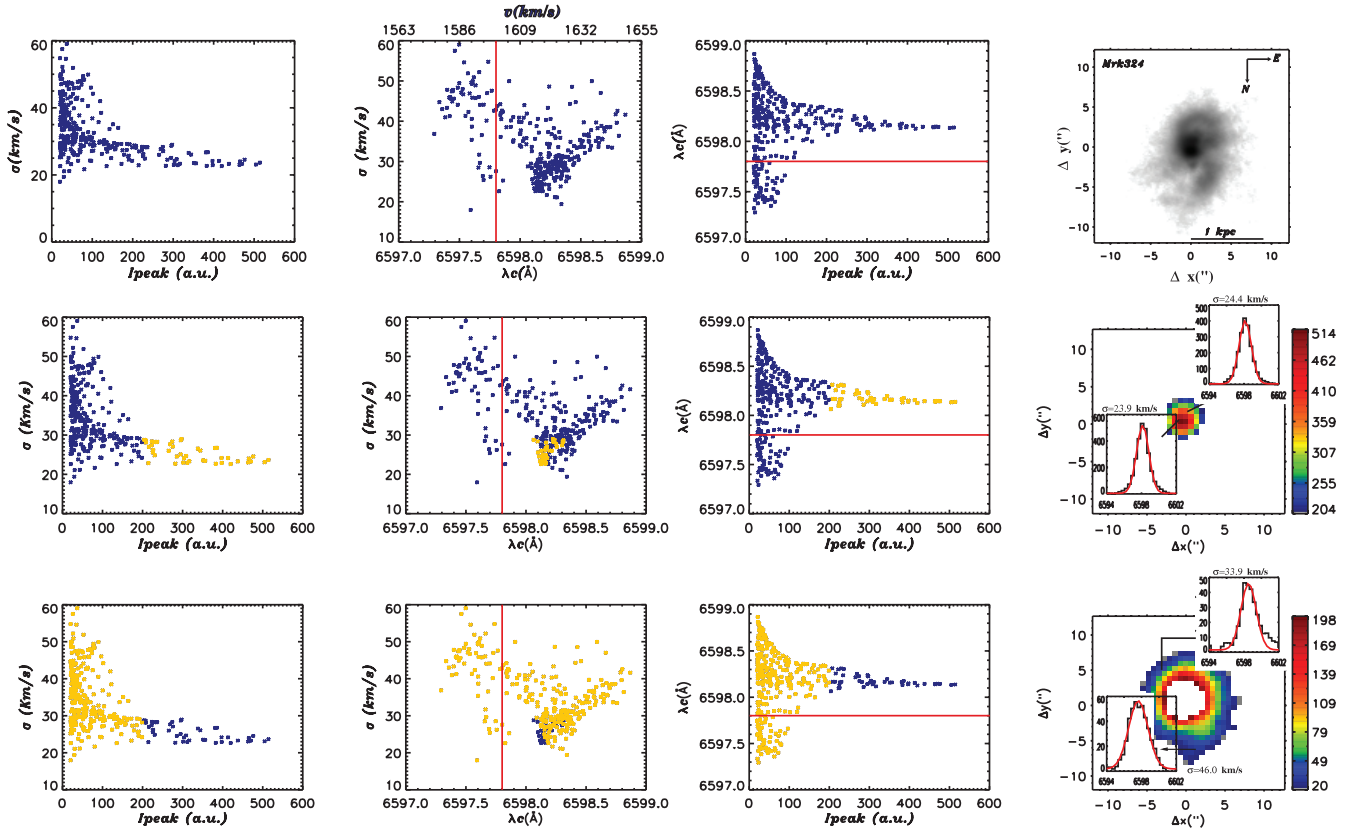

FIG. 1.— *Top row*: Velocity dispersion σ vs. peak intensity (the σ was corrected for the instrumental and thermal broadening) for all the Gaussian fits to the individual spectra of Mrk 324. The second and third panels display the corresponding σ vs. central lambda (λ_c; indicated also is the velocity range in kilometers per second) and λ_c vs. peak intensity, respectively. The solid line in these two panels indicates the rest velocity of the galaxy. The last panel shows the Hα image of the galaxy and indicates its scale in kiloparsecs. *Middle and bottom rows*: Highlighted in color are the various sets of data points selected in the σ vs. peak intensity diagram and their locations in the σ vs. λ_c and λ_c vs. peak intensity planes. The last panels in each row, with a peak intensity scale, display the locations in the galaxy that produce the selected data points. Insets in these panels correspond to typical Gaussian fits (*red solid lines*) to the data, arising from different regions (axes correspond to intensity, in counts, and the wavelength, in angstroms). The fitted σ-values are indicated in each frame.

(see Cairós et al. 2001) obtained at the 2.2 m telescope of the Centro Astronómico Hispano Alemán (CAHA) at the Calar Alto Observatory (Spain). The ionized gas in Mrk 370 (see the Hα image in Fig. 2) presents much more structure than Mrk 324. However, its σ versus $I_{\rm peak}$ diagram looks almost identical to that shown in Figure 1 for Mrk 324. The only exception is perhaps the low-intensity data points with values of σ below the supersonic lower limit imposed by the horizontal band ($\leq$21 km s^{-1}; see Fig. 2, *top left panel*). The structure of the photoionized gas in Mrk 370 begins to be disentangled when one selects the data from the horizontal band in the σ versus $I_{\rm peak}$ diagram (see Fig. 2, *second row*). Such a data set appears clumped at three different λ_c values in the σ versus λ_c diagram. The brightest one sits at the rest wavelength of the galaxy (6580.1 Å). There is a second one at $\sim$6579.4 Å and a third one between these two, at $\sim$6579.8 Å. Two of them are much more apparent in the λ_c versus $I_{\rm peak}$ diagram, in which they clearly end up as pointed structures with different intensities (factors of 2) and different central wavelengths. The emission-line peak intensity map tracing the selected points (Fig. 2, *second row, right panel*) shows two major bursts of stellar formation and two adjacent, much less intense bursts associated with the massive central stellar clusters with masses in the range $(8-50)\times10^4\,M_\odot$ (see Martínez-Delgado 2005; Martínez-Delgado et al. 2006), also resolved by Cairós et al. (2002) using the INTEGRAL spectrograph with a single-Gaussian fit to the emission lines. All of these, although near the center of the galaxy, are kinematically resolved as well-detached structures. This multiplicity of structures would have been missed if one had used only the σ versus $I_{\rm peak}$ diagram as a diagnostic for this galaxy (see Fig. 2, *top left panel*), as the brightest points present almost the same supersonic Gaussian profiles. These massive regions also match the area of the galaxy that shows the highest ionization values (see the Hα emission line and the [O III]/Hβ maps in Cairós et al. 2002).

The third row of panels in Figure 2 displays the data from the inclined bands with low-intensity and large σ-values in the σ versus $I_{\rm peak}$ diagram. This data set, like the corresponding one in Mrk 324, presents a large range of values of λ_c around the systemic velocity of the galaxy. The spread of the data is also noticeable in the λ_c versus $I_{\rm peak}$ plane. The bulk of the data arise from a large galactic volume shown in the emission-line peak intensity map as an expanding rim of gas around the main centers of star formation all over the galaxy. This is most intense around the nuclear starburst zone and although less intense, it is still noticeable around smaller bursts of stellar formation some 2 kpc away from the nuclear region.

The bottom row of panels shows the low-intensity and low-velocity-dispersion data from the σ versus $I_{\rm peak}$ diagram (see Fig. 2), which appears as vertical well-detached low-σ structures in the σ versus λ_c plane. These structures, given their low values of σ, detach well from the bulk of the data, most of which present supersonic values, and due to their very different λ_c values they also appear as well-detached entities along the λ scale. Note, however, that given their low-intensity values, they are much less

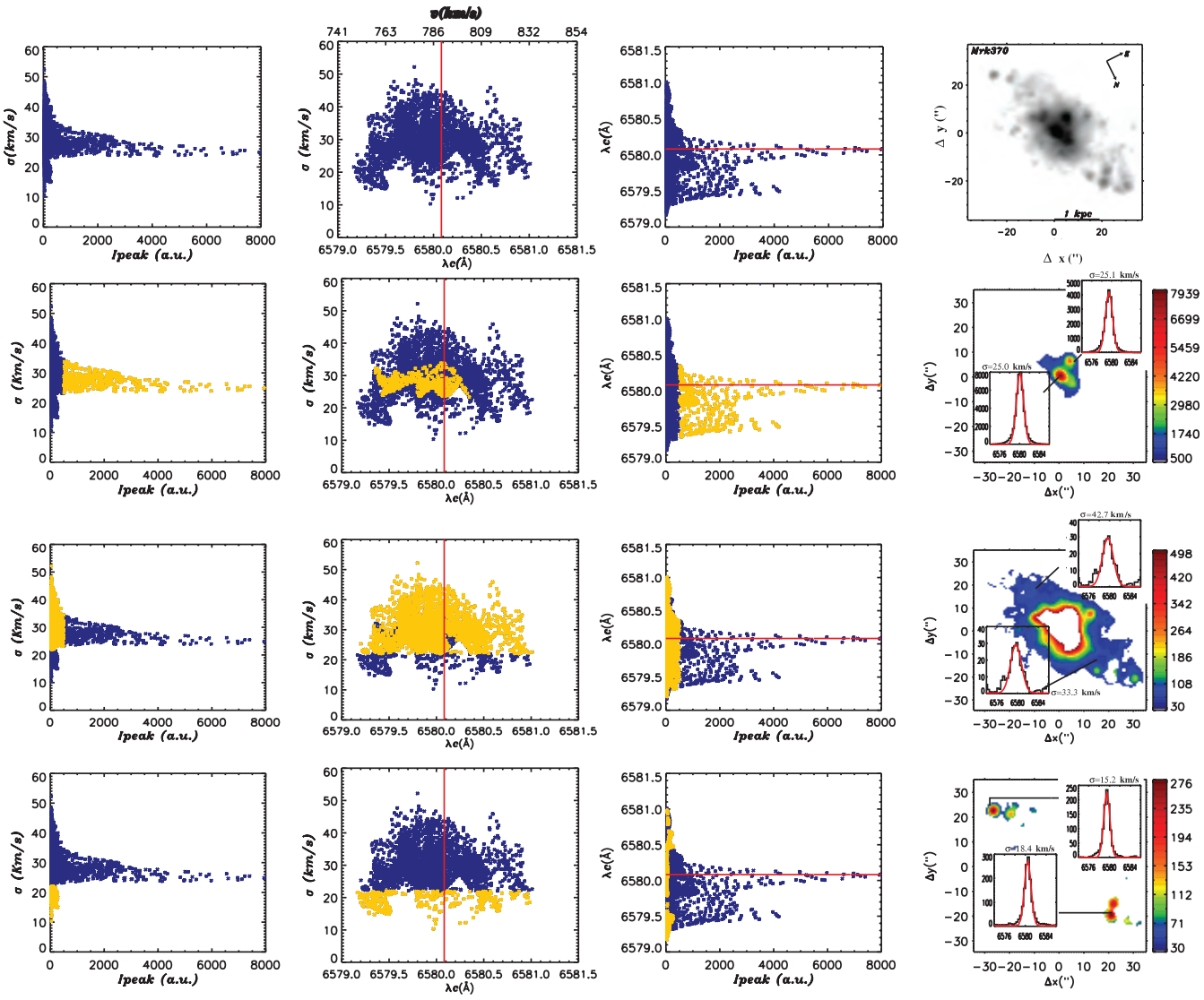

FIG. 2.—Same as Fig. 1, but for Mrk 370.

apparent in the λ_c versus $I_{\rm peak}$ diagram. These data points correspond in the emission-line peak intensity map (Fig. 2, *bottom right panel*) to multiple knots of emitting gas, or H II regions excited by low-mass stellar groups (with masses $\leq 10^4\ M_\odot$; see Martínez-Delgado 2005; Martínez-Delgado et al. 2006) at large distances from the center of the galaxy. The line profiles arising from these regions are also Gaussian profiles, although with very low intensity when compared to those arising from the central starburst regions (see the insets in Fig. 2, *last column*).

3.3. *III Zw 102*

This galaxy is believed to be the result of an interaction event (see Vorontsov-Velyaminov 1959, 1977) and has been considered by some authors to belong to the polar-ring galaxy type (Whitmore et al. 1990). It is morphologically considered an extended BCG (Cairós et al. 2001), in which 65 star-forming regions spread over the whole main body of the galaxy, including the arms, have been identified. The age of the knots and their low age dispersion (6.1 ± 0.6 Myr) suggest a coeval starburst event (see Martínez-Delgado et al. 2006).

Figure 3 displays the results for III Zw 102. The top right panel shows the Hα image of the extended galaxy (see Cairós et al. 2001) obtained at the NOT 2.52 m telescope of the ORM in La Palma (Spain).

The data for III Zw 102 confirm the power of all the diagnostic diagrams used here. The galaxy has a plethora of small H II regions spread along two arms, as well as several massive centers of stellar formation in the densest nuclear region with masses of $\sim 10^5$–$10^6\ M_\odot$ (see Martínez-Delgado 2005; Martínez-Delgado et al. 2006). All of these, as well as the large galactic volumes undergoing a supersonic expansion, leave their signature in the diagnostic diagrams. In this way, the horizontal band with supersonic σ-values at all possible intensities noticeable in the σ versus $I_{\rm peak}$ diagram (see Fig. 3, *second row*) is spread over a large range of λ_c values in the σ versus λ_c diagram and into at least four pointed structures (at $\lambda_c = 6596.7$, 6597.25, 6598, and 6600 Å) of different intensities in the λ_c versus $I_{\rm peak}$ diagram. All of these points in the emission-line peak intensity map are well resolved as giant structures within the galactic nuclear region. On the other hand, the larger σ-points at all peak intensities in the σ versus $I_{\rm peak}$ diagram arise from gas expanding around the nuclear zone (see Fig. 3, *third row*). Among this data set is the inclined structure between $I_{\rm peak} = 1100$ and 1400, which is produced by gas between the four major centers of stellar formation in the

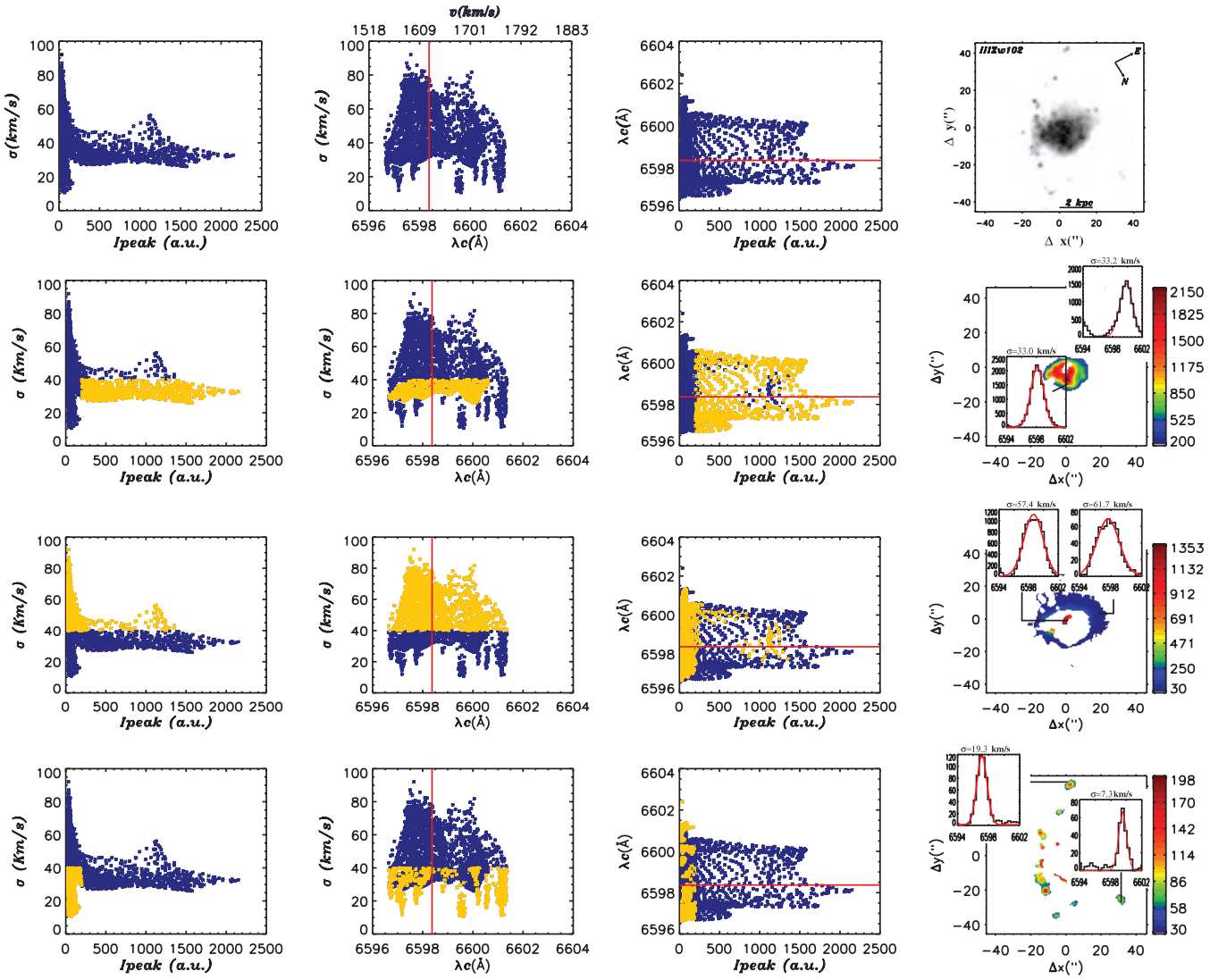

FIG. 3.—Same as Fig. 1, but for III Zw 102.

nuclear region. The broad line structure appears at the center of the galaxy, with a λ_c value very similar to the systemic velocity of III Zw 102.

Finally, the lowest σ and lowest intensity data points in the σ versus $I_{\rm peak}$ diagram (Fig. 3, *bottom row*) appear, as in the case of Mrk 370, as a set of well-detached vertical stalactites in the σ versus λ_c diagram, hanging from the bulk of the data at very distinct λ_c values, and they are produced by the small H II regions located along the galactic arms (see Fig. 3, *bottom right panel*). As shown by the insets in the last column of panels, the quality of the Gaussian fits is totally different in the three regions. The nuclear zone shows supersonic perfect Gaussians, while the surrounding gas presents much broader and asymmetric lines. Single Gaussians with small σ-values fit well the data from small centers of star formation.

4. SUMMARY

Three-dimensional spectroscopy with good spatial and spectral resolution, sampling a particular emission line over the whole area covered by an emitting nebula, is known to be the most suitable observational technique for analyzing the global kinematics of GHIIRs. In particular, if a single-Gaussian fit is carried out over the emission lines in every pixel, one could infer the velocity dispersion, central wavelength, and peak intensity of the lines. The resultant σ versus $I_{\rm peak}$ diagram (Muñoz-Tuñón et al. 1996) has been shown to be an excellent diagnostic diagram to separate the main broadening mechanisms affecting the emission lines: e.g., those that lead to shells and loops generated by the violent action from massive stars (see Dyson 1979; Roy et al. 1986), which finally lead to cloud dispersal, and those affecting the regions of massive star formation (either gravity [see Terlevich & Melnick 1981; Tenorio-Tagle et al. 1993] or turbulence [see Chu & Kennicutt 1994]). The sequences shown by the various GHIIRs so far analyzed led the authors also to propose the σ-$I_{\rm peak}$ plot as a tool able to trace the evolutionary status of a GHIIR from its formation to the total dispersal of the ionized gas.

Here we have confirmed that the data from the inclined supersonic bands in the σ versus $I_{\rm peak}$ diagrams are caused by the mechanical energy deposited by massive stellar sources. These sources, depending on the age of the stellar clusters and on the density of the surrounding gas, may affect small or large galactic volumes. However, in all cases, the interaction leads to very asymmetric line profiles, evident in the σ versus $I_{\rm peak}$ diagram for their highly supersonic σ-values.

Here we have extended the analysis to blue compact galaxies. We have selected sources with a single nuclear starburst (such as Mrk 324), as well as galaxies with multiple stellar bursts both within their nuclei and at large galactocentric distances. In all

cases the σ versus I_{peak} diagram resembles those from GHIIRs in which the data define a supersonic σ (larger than $c_{H\,II} \approx 10$ km s^{-1}) horizontal band with all possible intensity values. Note that the value of the limiting σ is different in each case. For III Zw 102 the horizontal band peaks at $\sim$33 km s^{-1}, while for Mrk 324 and Mrk 370 it occurs at 24 and 25 km s^{-1}, respectively.

The σ horizontal band, for the case of multiple massive nuclear bursts of stellar formation, has been shown to split into different bands in the λ_c versus I_{peak} diagram. In this new diagram, the largest nuclear regions of massive star formation become evident due to the good spectral resolution. Thus, even with a poor spatial resolution or when dealing with sources farther away, the sampling of the velocity field with our three-dimensional spectrographs would reveal the exciting sources. Similarly, the new σ versus λ_c diagram picks up the small bursts of stellar formation by tracing their lower intensity and the slower expansion of their immediate surroundings.

The stalactites detected in the σ versus λ_c diagram in the case of III Zw 102 and Mrk 370 correspond to the ionized knots located in the outskirts of the galaxies, and their spread in σ results from the H II regions' expansion into a low-density medium (see Franco et al. 1990).

Overall, the new diagnostic diagrams presented here provide the possibility of inferring from three-dimensional spectroscopy the magnitude of the star formation activity of distant galaxies, even if they are not spatially resolved.

I. M.-D. acknowledges an FPI grant (FP-2001-2506) from the Spanish government through the collaboration of project AYA2004-08260-C03-01 (ESTALLIDOS; see http://www.iac.es/project/GEFE/estallidos). A. V. M. acknowledges the Russian Foundation for Basic Research (project 05-02-16454). This work is partly based on observations carried out at the 6 m telescope of the Special Astrophysical Observatory of the Russian Academy of Sciences, operated under the financial support of the Science Department of Russia (registration No. 01-43), and it has been partly supported by ESTALLIDOS project AYA2004-08260-C03-01 and grant AYA2004-02703 from the Spanish Ministerio de Educación y Ciencia.

REFERENCES

Afanasiev, V. L., & Moiseev, A. V. 2005, Astron. Lett., 31, 194
Cairós, L. M., Caon, N., García-Lorenzo, B., Vílchez, J. M., & Muñoz-Tuñón, C. 2002, ApJ, 577, 164
Cairós, L. M., Caon, N., Vílchez, J. M., Gónzalez-Pérez, J. N., & Muñoz-Tuñón, C. 2001, ApJS, 136, 393
Chu, Y.-H., & Kennicutt, R. C., Jr. 1994, ApJ, 425, 720
Dyson, J. E. 1979, A&A, 73, 132
Franco, J., Tenorio-Tagle, G., & Bodenheimer, P. 1990, ApJ, 349, 126
Fuentes-Masip, O., Muñoz-Tuñón, C., Castañeda, H. O., & Tenorio-Tagle, G. 2000, AJ, 120, 752
Martínez-Delgado, I. 2005, M. S. thesis, Univ. La Laguna, Instituto de Astrofísica de Canarias, Spain
Martínez-Delgado, I., Muñoz-Tuñón, C., Cairós, L. M., & Tenorio-Tagle, G. 2006, AJ, submitted
Moiseev, A. V. 2002, Bull. Spec. Astrophys. Obs., 54, 74
Muñoz-Tuñón, C. 1994, in Violent Star Formation from 30 Doradus to QSOs, ed. G. Tenorio-Tagle (Cambridge: Cambridge Univ. Press), 25
Muñoz-Tuñón, C., Gavryusev, V., & Castañeda, H. O. 1995, AJ, 110, 1630
Muñoz-Tuñón, C., Tenorio-Tagle, G., Castañeda, H. O., & Terlevich, R. 1996, AJ, 112, 1636
Roy, J.-R., Arsenault, R., & Joncas, G. 1986, ApJ, 300, 624
Sabalisck, N. S. P., Tenorio-Tagle, G., Castañeda, H. O., & Muñoz-Tuñón, C. 1995, ApJ, 444, 200
Telles, E., Muñoz-Tuñón, C., & Tenorio-Tagle, G. 2001, ApJ, 548, 671
Tenorio-Tagle, G., Muñoz-Tuñón, C., & Cox, D. P. 1993, ApJ, 418, 767
Terlevich, R., & Melnick, J. 1981, MNRAS, 195, 839
Thuan, T. X., & Martin, G. E. 1981, ApJ, 247, 823
Vorontsov-Velyaminov, B. A. 1959, Atlas and Catalog of Interacting Galaxies (Moscow: Moscow State Univ.)
———. 1977, A&AS, 28, 1
Whitmore, B. C., Lucas, R. A., McElroy, D. B., Steiman-Cameron, T. Y., Sackett, P. D., & Olling, R. P. 1990, AJ, 100, 1489